https://doi.org/10.5194/essd-2022-45
Preprint. Discussion started: 1 March 2022

Open Access Earth System Science Data Discussions

1km Monthly Precipitation and Temperatures Dataset for China from 1952 to 2019 based on a Brand-New and High-Quality Baseline Climatology Surface

Haibo Gong[1, 2, 3, 4, 5], Huiyu Liu* [1, 2, 3, 4, 5], Xueqiao Xiang[1, 2, 3, 4, 5], Fusheng Jiao[1, 2, 3, 4, 5]
Li Cao[1, 2, 3, 4, 5], Xiaojuan Xu[1, 2, 3, 4, 5],

[1]Jiangsu Center for Collaborative Innovation in Geographical Information Resource Development and Application, Nanjing Normal University, Nanjing, 210023, China
[2]Key Laboratory of Virtual Geographic Environment (Nanjing Normal University), Ministry of Education, Nanjing, 210023, China
[3]State Key Laboratory Cultivation Base of Geographical Environment Evolution (Jiangsu Province), Nanjing Normal University, Nanjing, 210023, China
[4]College of Geography Science, Nanjing Normal University, Nanjing 210023, China
[5]Jiangsu Key Laboratory of Environmental Change and Ecological Construction, Nanjing Normal University, Nanjing 210023, China

Correspondence: Dr Huiyu Liu, Nanjing Normal University, No 1 Wenyuan Road, Qixia District, Nanjing, China. Tel: (+86) 18951838599; E-mail: liuhuiyu@njnu.edu.cn

https://doi.org/10.5194/essd-2022-45
Preprint. Discussion started: 1 March 2022

Abstract

Long-term climate data and high-quality baseline climatology surface with high resolution are essential to multiple fields including climatological, ecological, and environmental sciences. Here, we created a brand-new baseline climatology surface (ChinaClim_baseline) and developed a 1km monthly precipitation and temperatures dataset in China during 1952-2019 (ChinaClim_time-series). Thin plate spline (TPS) algorithm in each month with different model formulations by accounting for satellite-driven products and climatic research unit (CRU) datasets, was used to generate ChinaClim_baseline and monthly climate anomaly surface. Climatologically aided interpolation (CAI) was used to superimpose monthly anomaly surface with ChinaClim_baseline to generate ChinaClim_time-series. Our results showed that ChinaClim_baseline exhibited very high performance in four climatic regions with the *RMSEs* of precipitation and temperature elements estimation being 1.276 ~28.439 mm and 0.310 ~ 2.040 °C, respectively. The correlations among ChinaClim_baseline and WorldClim2 and CHELSA were high, but our results also captured clearly spatial differences among them. WorldClm2 and CHELSA might overestimated (or underestimated) climate events such as warming and drought in temperate continental region and high cold Tibetan plateau where weather stations were sparse. For ChinaClim_time-series, precipitation and temperature elements had average *RMSEs* between 7.502 mm ~ 52.307 mm, and 0.461 °C ~ 0.939 °C for all months, respectively. Compared with Peng's climate surface and CHELSAcruts, R^2 increased by ~ 7 %, *RMSE* and *MAE* decreased by ~ 17 % for precipitation; for temperature elements, R^2 hardly increased, but *RMSE* and *MAE* decreased by ~50 %. Our results showed ChinaClim_baseline obviously improved the accuracy of time-series climatic elements estimation, and the satellite-driven data can greatly improve the accuracy of time-series precipitation estimation, but not the accuracy of time-series temperatures estimation. Overall, ChinaClim_baseline, an excellent baseline climatology surface, can be used for obtaining high-quality and long-term climate datasets from past to future. In the meantime, ChinaClim_time-series of 1km spatial resolution based on ChinaClim_baseline, is suitable for investigating the spatial-temporal patterns of climate changes and their impacts on eco-environmental systems in China.

Here, ChinaClim_baseline is available at 10.5281/zenodo.5900743 (Gong, 2020a), ChinaClim_time-series of precipitation is available at 10.5281/zenodo.5919442 (Gong, 2020b), ChinaClim_time-series of maximum temperature is available at 10.5281/zenodo.5919448 (Gong, 2020c), ChinaClim_time-series of minimum temperature is available at 10.5281/zenodo.5919423 (Gong, 2020d) and ChinaClim_time-series of average temperature is available at 10.5281/zenodo.5919450 (Gong, 2020e).

https://doi.org/10.5194/essd-2022-45
Preprint. Discussion started: 1 March 2022

1 Introduction

Long-term information on climatic conditions with high resolution (1km) is pivotal for understanding climate changes and its influences in atmospheric movements, vegetation dynamics, soil water content , and other related scientific and application fields (Chaney et al., 2014; Gao et al., 2018; Hijmans et al., 2005; Karger et al., 2017; Liu et al., 2016; New et al., 2002; Pfister et al., 2020; Wagner and Wolfgang, 2003). However, existing climate datasets often only represent climatic variation at spatial resolutions of 0.25~1 degree, such as Climatic Research Unit: CRU (Harris et al., 2014), The European Centre for Medium-Range Weather Forecast (ECWMF) Climatic reanalysis: ERA (Sterl et al., 1998), Global Precipitation and temperature: UDEL (Lawrimore et al., 2011), The Berkeley Earth Surface Temperatures: BEST (Muller et al., 2013), Global Precipitation Climatology Centre: CPCC (Becker et al., 2013). As the studying of climate change and its regional responses becomes more and more important, high resolution gridded climate data is urgently needed for national and regional scales (Hamann et al., 2015; Hijmans et al., 2005; Karger et al., 2017).

A large body of works including spatial interpolation methods and statistical downscaling were motivated to obtain high resolution gridded climate data. Spatial interpolation methods such as Kriging (Li and Shao, 2010; Wu and Li, 2013), Inverse Distance Weighting (Hartkamp et al., 1999) and Spline (Boer et al., 2001) were widely applied in estimating climate elements (temperatures, precipitation, vapor pressure, solar radiation and wind speed) at arbitrary spatial resolution. Among them, thin plate spline (TPS) interpolation was considered to perform well in generating grids of climate elements (Boer et al., 2001; Hartkamp et al., 1999; Hijmans et al., 2005; Hutchinson, 1995; Fick et al., 2017). Recent studies have shown that climatologically aided interpolation (CAI) employing the temporal anomaly (ratio) surface and an accurate baseline climatology surface, is well suited for producing more high-quality climate datasets than direct interpolation using original weather stations (Abatzoglou et al., 2018; Becker et al., 2013; C. Vega et al., 2017; Karger et al., 2017; Mosier et al., 2014; Peng et al., 2019; Willmott and Robeson, 2010). Remarkably, the quality of monthly time-series climate surface, generated by CAI method, was highly determined by the baseline climatology surface (Gao et al., 2018; Peng et al., 2019). Baseline climatology surface, also called 30-Year Normals, described average monthly conditions over the most recent three full decades. Fine-scale baseline climatology surface is physically representative and meaningful meteorological variable for climatology studies (Marchi et al., 2019; Mosier et al., 2014; Peng et al., 2017; Platts et al., 2015). Previous efforts have developed some high-quality baseline climatology surfaces with a resolution of 1km, such as WorldClim v1 (Hijmans et al., 2005), WorldClim2 (Fick et al., 2017) and CHELSA (Karger et al., 2017) for global land surface, PRISM (Daly et al., 2002; Daly et al., 2008) and Daymet (Thornton et al., 1997) for North America. Although these baseline climatology surfaces are widely used for basic and applied studies (Belda et al., 2017; Ray et al., 2015), a gap between these gridded climate datasets and weather stations was still observed in many areas (New et al., 2002; Fick et al., 2017). For example, data quality of WorldClim depends on local climate variability, quality and density of observations, and the degree of the fitted spline (Hijmans et al.,2005). Unfortunately, currently available high-quality baseline climatology surface with high-resolution covering China like WorldClim2 and CHELSA, only a part of weather stations (323 and 228 stations for WorldClim2 and CHELSA respectively) were employed to generate baseline

https://doi.org/10.5194/essd-2022-45
Preprint. Discussion started: 1 March 2022

climatology surface. Weather stations are the most reliable source of the estimation of temperatures and precipitation, and thus more weather stations can provide more accurate point measure information. Thus, a dataset of 30-year average climate (1981-2010) containing more than 2000 weather stations from China Meteorological Data Service Center and Central Weather Bureau, can be used to create a brand-new baseline climatology surface in China. Notably, CHELSA have not considered satellite-driven products, and WorldClim2 did not use directly satellite-driven precipitation products but cloud cover datasets as predictor. However, satellite-driven products can improve the estimate of climate elements in the regions with less regular distribution of meteorological stations (Deblauwe et al., 2016; Jin and Dickinson, 2010; Mildrexler et al., 2011). With the development of remote sensing and geographic information technology, satellite-driven climate grid become the optimum climate product in measuring climate elements at regional and global scales (Huffman et al., 2010; Michaelides et al., 2009; Siuki et al., 2017). The Multisatellite Precipitation Analysis monthly 3B43 products (TRMM3B43) have been utilized extensively to provide valuable precipitation information in areas with sparse weather stations over the last two decades (Biasutti et al., 2012; Huffman et al., 2010; Simpson et al., 1996). Land surface temperature (LST) is now available from satellite-borne instruments, which is widely incorporated in estimating air temperature (Kilibarda et al., 2014, Yao et al., 2020). Despite TRMM3B43 and LST products played huge roles in recent precipitation and temperature measures (Kilibarda et al., 2014; Kolios and Kalimeris, 2020; Yao et al., 2020), they are only available after 1997 and 2000 respectively, which is not long enough for the long-term ecological and environmental analyses and modeling. Therefore, there is an urgently need to combine satellite-driven TRMM3B43 and LST in climate interpolation to generate a brand-new and higher-quality baseline climatology surface (ChinaClim_baseline) and further to create a high-quality monthly time series of precipitation and temperatures dataset for China (ChinaClim_time-series) from 1952 to 2019 with CAI method. Specifically, the objectives of this work are: (1) to create a brand-new and higher-quality baseline climatology surface for China (ChinaClim_baseline). (2) to generate a 1km monthly temperatures and precipitation dataset in China for the period of 1952-2019 (ChinaClim_time-series).

https://doi.org/10.5194/essd-2022-45
Preprint. Discussion started: 1 March 2022

Open Access Earth System Science Data Discussions

2 Data

2.1 Weather observation stations

Dataset of 30-year average climate (1981-2010) was obtained from two sources, 2438 weather stations from CMD and 25 weather stations from Central Weather Bureau (www.cwb.gov.tw). Dataset of monthly surface observation values drawn from 613 weather stations for the period of 1952-2019 was collected from the China Meteorological Data Service Center (CMD: http://cdc.nmic.cn). Moreover, influenced by the monsoon and Tibetan Plateau, four climate regions (Figure 1: Temperate continental region, Temperate monsoonal region, High cold Tibetan Plateau, and Subtropical-tropical monsoonal region) have experienced various climate changes in both precipitation and temperature (He et al 2018). Weather stations also were divided into four regions to construct model and check the performance of data products in the areas with sparse and dense weather stations.

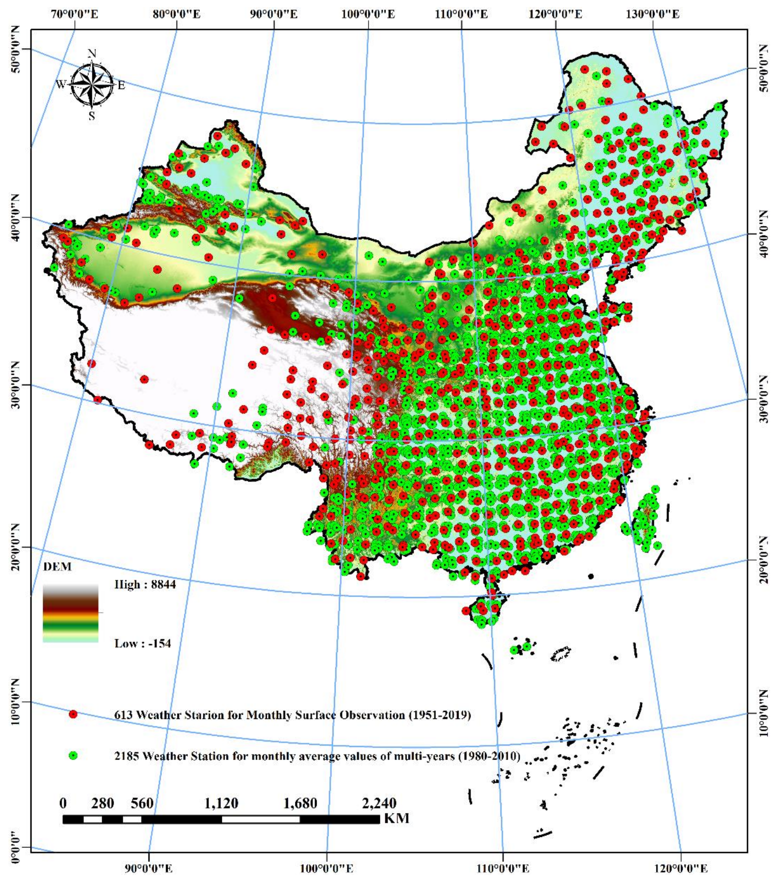

Figure1. The spatial distribution of weather stations in four climatic regions (i.e. Temperate continental region, Temperate monsoonal region, High cold Tibetan plateau, and Subtropical-tropical monsoonal region) of China.

https://doi.org/10.5194/essd-2022-45
Preprint. Discussion started: 1 March 2022

2.2 Version 7 TRMM3B43 datasets

The Tropical Rainfall Measuring Mission (TRMM), a joint project by the National Aeronautics and Space Administration (NASA) and the Japan Aerospace Exploration Agency (JAXA), was launched in November 1997 to monitor and investigate tropical and subtropical rain system (Huffman et al., 2010; Simpson et al., 1996). Our study used the TRMM3B43 monthly product, with a spatial resolution of 0.25 degree over a latitude range from 50°S to 50°N. The Version 7 monthly TRMM3B43 in NetCDF format was downloaded from https://mirador.gsfc.nasa.gov. Referring to the method of Ma et al (2018), monthly and yearly TRMM3B43 (TRMM_m and TRMM_y) were averaged across years 1998-2019 by downscaled to 1km spatial resolution via cubist algorithm and TPS interpolation.

2.3 Land Surface Temperature

Land surface temperature (LST) was compiled from Moderate Resolution Imaging Spectroradiometer (MODIS). Mean night and day LST values were extracted from ~1 km resolution MOD11A2 images, averaged by month and year from 2001 to 2019. Then, the night LST (lst_nm /lst_ny) was used as either covariates or independent spline variables for minimum temperature, the day LST (lst_dm/lst_dy) was used as either covariates or independent spline variables for maximum temperature and an average of lst_dm/lst_dy and lst_nm/lst_ny (lst_am/ lst_ay) was used as either covariates or independent spline variables for average temperature.

2.4 Elevation and Distance to the nearest coast

Elevation data with a spatial resolution of 90 m from Shuttle Rader Topography Mission (SRTM) (data available at http://srtm.csi.cgiar.org/) was aggregated to 1km spatial resolution. Precipitation generally increases with elevation (Oke, 1978; Barry and Chorley, 1987), and temperature exhibits a predictable decrease with elevation when the atmosphere is well mixed (e.g. Willmott and Matsuura, 1995). Coastline dataset was downloaded from https://www.ngdc.noaa.gov. Coastal effects on temperatures and precipitation are most noticeable because the water temperature is significantly different from the adjacent land temperature and ocean often brings warm-humid water vapor (Haugen and Brown, 1980; Atkinson and Gajewski, 2002). We calculated the distance to the nearest coast using Euclidean distance in ArcGIS 10.2 with the fine coastline datasets.

2.5 Climatic Research Unit gridded Time Series (CRU TS v. 4.05)

Climatic Research Unit gridded Time Series (CRU TS) is a widely used climate dataset on a 0.5° ×0.5° grid over all land domains of the world except Antarctica. The new version (CRU TS v4) was updated to span 1901–2018 by the inclusion of additional station observations, and it will be updated annually. CRU TS v. 4.05 can be accessed online at https://crudata.uea.ac.uk/cru/data/hrg/. Although the coarse spatial resolution of CRU dataset, it can provide valuable information on the

https://doi.org/10.5194/essd-2022-45
Preprint. Discussion started: 1 March 2022

time-varying characteristics of climatic elements. Here, we calculated the CRU anomaly (ratio) during 1952-2019 and interpolated them to 1km spatial resolution via TPS algorithm as variable for monthly temperatures anomaly (precipitation ratio) estimation.

2.6 Baseline climatology surfaces and monthly time-series climatic datasets

Two baseline climatology surfaces as WorldClim2 (Fick et al., 2017) and CHELSA (Karger et al., 2017) with 1km spatial resolution were used to compare the spatial consistency with ChinaClim_baseline. WorldClim2 was interpolated with ANUSPLIN (Hutchinson, 1995) and represented the period of 1970-2000, a method that fits thin plate splines through station data in three dimensions: latitude, longitude, and elevation. WorldClim2 data sets can be accessed online at www.worldclim.org. CHELSA contains high spatial resolution monthly climatologies of average, maximum, and minimum temperatures and precipitation, representing the period of 1979-2013. CHELSA is essentially a quasi-mechanistical statistical downscaling of the ERA-Interim reanalysis, with the temperature downscaling based on mean lapse rates and elevation, and the precipitation algorithm using geographic predictors including wind fields, exposure, and boundary layer height (Karger et al., 2017). CHELSA is freely available at www.chelsa-climate.org.

We also collected two long-term climate datasets with high resolution. One is CHELSAcruts, a delta changes monthly climate dataset for the years 1901-2016 for mean monthly maximum temperatures, mean monthly minimum temperatures, and monthly precipitation sum. Anomalies of the CRU TS v. 4.01 dataset were interpolated between all CRU TS grid cells and are then added (for temperature variables) or multiplied (in case of precipitation) to high resolution climate data from CHELSA V1.2 (Karger et al., 2017). CHELSAcruts is freely available at www.chelsa-climate.org. The other is the recently published Peng's climate surfaces (Peng et al., 2019). This climate dataset was spatially downscaled from 30' CRU time series dataset with the baseline climatology surface of WorldClim using CAI method. This is a 1km dataset of monthly air temperatures at 2m and precipitation for China during the period of 1901-2017. Peng's climate surface can be freely available at www.zenodo.org.

https://doi.org/10.5194/essd-2022-45
Preprint. Discussion started: 1 March 2022

3 Method

3.1 Creation of baseline climatology surface over China (ChinaClim_baseline)

The monthly average values of precipitation and temperatures of multi-years (1980-2010) were interpolated with the thin plate spline (TPS) from R packages "fields". Spline models for the *N* observed data values z_i are fit as the following:

$$z_i = f(x_i) + a^T y_i + \lambda \qquad (i = 1, \ldots, N)$$

Where f is a smooth function of the spline independent variable x_i, a is a vector of linear coefficients for the independent covariates y_i. In this study, we considered longitude, latitude, elevation, distance to the nearest coast and satellite-driven variables to create baseline climatology surface over China based on TPS model. We listed climate elements and variables used in TPS model for estimating ChinaClim_baseline in Table 1. It is worth noting that longitude, latitude and elevation were set as spline independent variables and other variables were used as either independent spline variables or linear covariates. Especially, Elevation (m) was divided by 1000 following scaling recommendations by Hutchinson (1995). Precipitation values were square root transformed prior to fitting following recommendations by Hutchinson and Xu (2013). Moreover, TRMM3B43 contained a latitude range from 50°S to 50°N, so we constructed TPS model including TRMM3B43 in the area south of 50°N. Because the northernmost latitude of China is higher than 50°N, we constructed TPS models without TRMM3B43 in the area north of 49°N. Obvious differences may be appeared in the border area since different model formulas using in two areas. Thus, the 1° overlap area ensures that baseline climatology surface of the two areas can be better merged by weighting estimates inversely proportional to distance from each region's border (Hijmans et al., 2005; New et al., 2002). Similarly, this method also was used in fusing the boundaries of the four different climate regions.

Specifically, the process for generating ChinaClim_baseline based on the tenfold spatially stratified cross-validation approach can be described as follows (Figure 2):

(1) After removing duplicate and invalid weather stations, the remaining were split into 10 folds in each climate region to assure that there was enough training and testing data for each climate region to build and verify the model, and thus to avoid spatial autocorrelation.

(2) We randomly extracted 9 folds' weather stations in each climate region and combined them into a new training dataset. The remained were combined as testing dataset to valid the accuracy of model.

(3) 11 model for each month in each climatic region were tried using different combinations of variables to construct TPS model (Model formulations about longitude, latitude, elevation, distance to the nearest coast and satellite-driven TRMM and LST described in Table S1).

(4) The optimal model for each month in each climatic region was used by selecting only the model with the lowest average *RMSE* value, then fit full dataset to create final surfaces and merge the region of interest via inverse distance weighted method.

https://doi.org/10.5194/essd-2022-45
Preprint. Discussion started: 1 March 2022

Table 1. Climate elements and variables used in TPS model for creating baseline climatology and anomaly surface. Variables include longitude (x), latitude (y), elevation (z), distance to the nearest coast (coast), averaged monthly CRU precipitation ratio (cru_r) and temperature anomaly (cru_a) during 1952-2019, averaged monthly (trmm_m) and yearly (trmm_y) TRMM3B43 during 1998-2019, monthly TRMM ratio (trmm_r), MOD11A2 land surface temperature (the day LST, the night LST, and the average of the day and night LST) during 2001-2019 averaged by month (lst_dm, lst_nm, lst_am) and year (lst_dy, lst_ny, lst_ay), MOD11A2 land surface temperature anomaly during 2001-2019 (lst_da, lst_na, lst_aa), Baseline climatology surface (base_prep, base_tavg, base_tmax, base_tmin).

Climate elements	Unit	Variables used in TPS models
Precipitation	mm	x, y, z,coast,trmm_m,trmm_y
Minimum temperature	℃	x, y, z,coast, lst_nm, lst_ny
Maximum temperature	℃	x, y, z,coast, lst_dm, lst_dy
Average temperature	℃	x, y, z,coast, lst_am, lst_ay
Precipitation ratio	%	x, y, z,coast, cru_r, trmm_r(1998-2019), base_prep
Minimum temperature anomaly	℃	x, y, z,coast, cru_a, lst_na(2001-2019), base_tmin
Maximum temperature anomaly	℃	x, y, z,coast, cru_a, lst_da(2001-2019), base_tmax
Average temperature anomaly	℃	x, y, z,coast, cru_a, lst_aa(2001-2019), base_tavg

Note: x, y and z were set spline independent variables and other variables were used as either independent spline variables or linear covariates

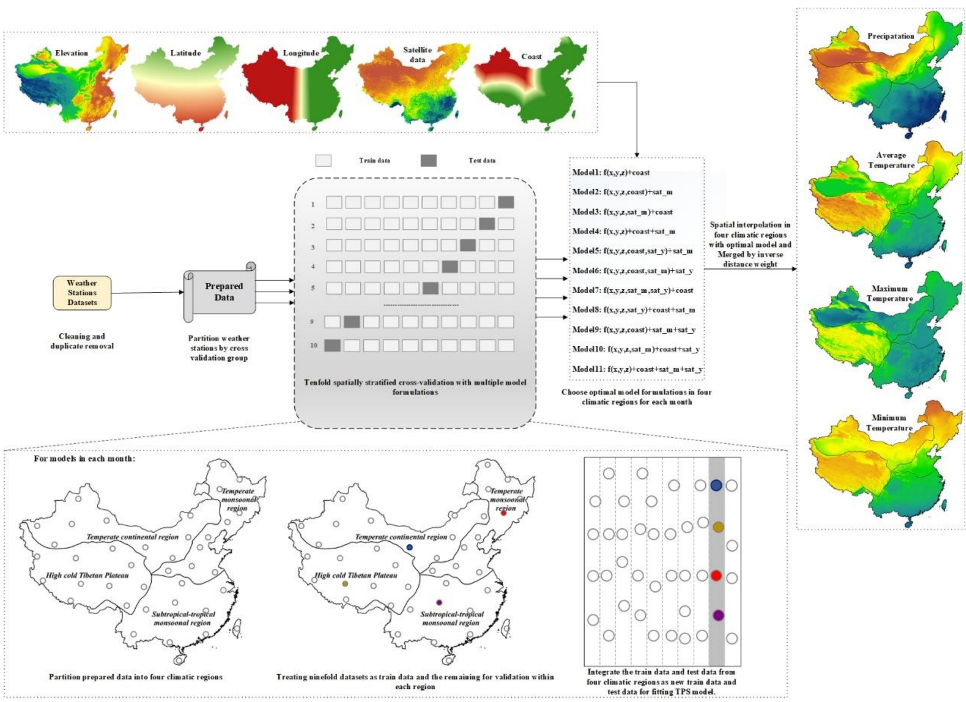

Figure 2. Workflow for baseline climatology surface (ChinaClim_baseline) for China (adapted from Fick et al., 2017)

https://doi.org/10.5194/essd-2022-45
Preprint. Discussion started: 1 March 2022

Open Access Earth System Science Data Discussions

3.2 Generation of monthly precipitation and temperatures surface for China (ChinaClim_time-series)

CAI method was used to superimpose monthly anomaly (ratio) surface and baseline climatology surface (ChinaClim_baseline) to produce monthly precipitation and temperatures surface (ChinaClim_time-series) during 1952-2019 in China as the following.

Firstly, the precipitation ratio and temperature anomaly time series were calculated by the ratio and the difference between the original time series from weather stations and the 30-Year Normals, respectively.

Secondly, we applied TPS model to generate monthly precipitation ratio and temperature anomaly surface from 1952.01 to 2019.12 with the similar way obtained ChinaClim_baseline (Figure 2). For monthly anomaly (ratio) during 1952-2019, 7 model formulations (Table S6) were constructed by using different combinations of variables (Longitude, Latitude, Elevation, Distance to the nearest coast, CRU anomaly (ratio) and the 30-Year normals), and the optimal model was chosen via the minimum *RMSE* value of multi-year (1952-2019) average to fit precipitation ratio surfaces during 1952-1997 and temperatures anomaly surfaces during 1952-2000; For the remained period, we also constructed two model formulations on the basis of the optimal model (1952-2019). The two models added satellite data (satellite-driven TRMM ratio and LST anomaly) as either independent spline variables or linear covariates. That is, 3 model formulations (eg: Table S6: model **1** was F(x,y,z,base,coast)+cru_r, model **1a** was F(x,y,z,base,coast)+cru_r+trmm_r and model **1b** was F(x,y,z,base,coast,trmm_r)+cru_r) were checked to select the best model during 1998-2019 for precipitation and 2001-2019 for temperature elements. Overall, The final anomaly/ratio surfaces were created by selecting only the model with the lowest average *RMSE* value in corresponding period.

Eventually, ChinaClim_time-series was generated by superimposing anomaly (ratio) time series grid and ChinaClim_baseline from 1952.01 to 2019.12 (Figure 3).

https://doi.org/10.5194/essd-2022-45
Preprint. Discussion started: 1 March 2022

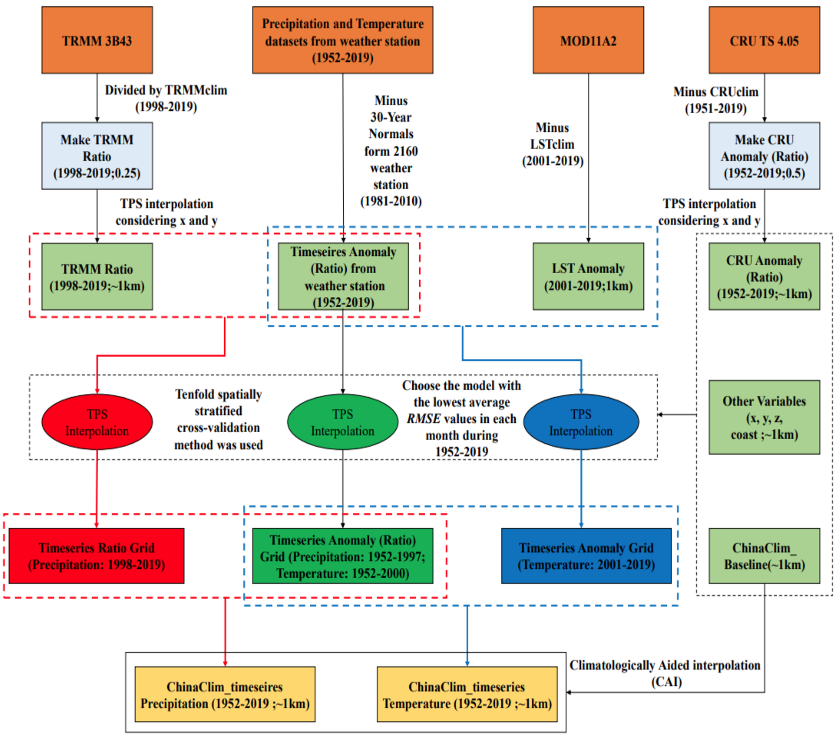

Figure 3. Workflow for ChinaClim_time-series generation.

3.3 Evaluation metrics

Three statistic indices including the root mean square error (*RMSE*), mean absolute error (*MAE*) and coefficients of determination (R^2) are examined to evaluate the performance of ChinaClim_baseline and ChinaClim_time-series.

$$RMSE = \sqrt{\frac{\sum_{i=1}^{n}(P_i - M_i)^2}{n}}$$

$$MAE = \frac{\sum_{i=1}^{n}|P_i - M_i|}{n}$$

$$R^2 = \left(\frac{\sum_{i=1}^{n}(M_i - \overline{M})(P_i - \overline{P})}{\sqrt{\sum_{i=1}^{n}(M_i - \overline{M})^2(P_i - \overline{P})^2}}\right)^2$$

Where *Pi* is the estimates like ChinaClim_baseline/ChinaClim_time-series in the *i*th weather station; *Mi* is the measured value from the *i*th weather station; *n* is the number of weather stations; $\overline{P}$ is the average of the estimates like ChinaClim_baseline/ChinaClim_time-series from *n* weather stations; $\overline{M}$ is the average of the measured value from *n* weather stations.

https://doi.org/10.5194/essd-2022-45
Preprint. Discussion started: 1 March 2022

Open Access Earth System Science Data Discussions

4 Results

4.1 A brand-new and high-quality baseline climatology surface for China (ChinaClim_baseline)

4.1.1 The optimal model and its overall accuracy

For precipitation estimation (Tables S2 - S5), the best model with the lowest RMSE from each region in each month employed satellite-driven TRMM3B43 (TRMM_m or TRMM_y), which implied that TRMM3B43 improved effectively precipitation accuracy. TRMM_m can improve the accuracy of precipitation in all months, while TRMM_y can only improve the accuracy in some months. Regardless of any region, the precipitation error in the summer half year was higher than that in the winter half year at month scale. The *RMSE* value of the summer half year was as high as 28.458mm in the Subtropical-tropical monsoonal region, followed by high cold Tibetan plateau and temperate monsoonal region, with *RMSE* of 15.708 and 15.572mm, respectively. However, precipitation error in temperate continental region was the lowest, and the highest *RMSE* in summer half year was just 8.694mm. Subtropical-tropical monsoonal region, high cold Tibetan plateau and temperate monsoonal region, strongly affected by monsoon, have abundant precipitation in the summer half year which tended to trigger higher precipitation error.

For all temperature elements (Tables S2 - S5), models considering LST were best in most months due to a strong correlation of temperature with LST in these months. That is, LST could improve the interpolation of temperatures, while the improvement by LST might be limited in some months over a specific region. For example, Model **1** (F(x,y,z)+coast) in Jul, Sep, Oct, Nov, and Dec were the best model for maximum temperature in temperate continental region, and it is the best model in 6 months (Jan, Feb, Apr, May, Sep, Oct) for minimum temperature in high cold Tibetan plateau. It means that temperature elements have very high correlation with altitude in related months over these regions and adding LST as an auxiliary variable is not necessary. As shown from Table.3, model accuracy was very high for the temperature elements when selecting the best model from each region in each month. Similar to precipitation, regardless of any region, the accuracy of temperature estimation in the summer half year was also higher than that of the winter half year, that is, compared with the winter half year, our results captured the lower *RMSE* and *MAE* for temperature elements in the summer half year. However, the temperature accuracy ranking of each temperature element was different over four climatic regions. In Temperate continental region and Temperate monsoonal region, the *RMSE* and *MAE* of the maximum temperature were the smallest, followed by the average and minimum temperature. In high cold Tibetan plateau and subtropical-tropical monsoonal region, the accuracy of the average temperature was the highest, followed by the maximum and minimum temperature. Specifically, the accuracy of average temperature in subtropical-tropical monsoonal region (an average *RMSE* between 0.369~0.632 ℃) was highest but close to that of temperate monsoonal region (an average *RMSE* between 0.310~0.732 ℃), followed by high cold Tibetan plateau (an average *RMSE* between 0.784~1.242 ℃) and temperate continental region (an average *RMSE* between 0.667~1.519 ℃). *RMSE* of the maximum temperature in

https://doi.org/10.5194/essd-2022-45
Preprint. Discussion started: 1 March 2022

temperate monsoonal region had an average *RMSE* between 0.273~0.452 ℃, followed by subtropical-tropical monsoonal region (an average *RMSE* between 0.475~0.798 ℃), temperate continental region (an average *RMSE* between 0.616~1.081 ℃), and high cold Tibetan plateau (an average *RMSE* between 0.990~1.509 ℃). For minimum temperature, the accuracy of temperature estimation in subtropical-tropical monsoonal region and temperate monsoonal region was good and had an average *RMSE* of 0.378~0.719 ℃ and 0.448~1.186 ℃, respectively, while the accuracy in high cold Tibetan plateau (an average *RMSE* of 0.893~1.853 ℃) and temperate continental region (an average *RMSE* of 0.893~1.853 ℃) was relatively poor.

Table 3. Tenfold cross-validation statistics for selected models based on independent weather stations in Temperate continental region

Climate elements	Statistic indices	Jan	Feb	Mar	Apr	May	Jun	Jul	Aug	Sep	Oct	Nov	Dec
Precipitation	*RMSE*	**1.367**	**1.276**	**2.316**	**4.679**	**6.663**	**6.759**	**8.694**	**7.226**	**4.873**	**3.628**	**2.574**	**1.603**
	R^2	0.848	0.823	0.779	0.750	0.791	0.894	0.935	0.960	0.941	0.851	0.842	0.893
	MAE	0.754	0.810	1.469	2.507	3.534	4.245	5.703	4.930	3.416	2.256	1.384	0.826
Average temperature	*RMSE*	**1.519**	**1.273**	**0.831**	**0.667**	**0.687**	**0.793**	**0.837**	**0.818**	**0.783**	**0.788**	**0.928**	**1.303**
	R^2	0.862	0.919	0.961	0.963	0.952	0.933	0.925	0.921	0.923	0.914	0.922	0.871
	MAE	1.003	0.842	0.593	0.479	0.470	0.544	0.581	0.572	0.570	0.582	0.690	0.889
Maximum temperature	*RMSE*	**1.081**	**1.030**	**0.846**	**0.616**	**0.702**	**0.750**	**0.802**	**0.733**	**0.663**	**0.607**	**0.727**	**0.980**
	R^2	0.936	0.949	0.964	0.974	0.956	0.952	0.942	0.951	0.959	0.964	0.956	0.935
	MAE	0.645	0.614	0.480	0.357	0.406	0.480	0.516	0.474	0.409	0.364	0.467	0.606
Minimum temperature	*RMSE*	**2.040**	**1.815**	**1.218**	**1.068**	**1.033**	**1.114**	**1.076**	**1.136**	**1.189**	**1.189**	**1.331**	**1.773**
	R^2	0.776	0.845	0.908	0.906	0.900	0.852	0.834	0.834	0.812	0.800	0.820	0.792
	MAE	1.457	1.286	0.916	0.826	0.806	0.854	0.813	0.843	0.914	0.879	1.013	1.285

Table 4. Tenfold cross-validation statistics for selected models based on independent weather stations in High cold Tibetan Plateau

Climate elements	Statistic indices	Jan	Feb	Mar	Apr	May	Jun	Jul	Aug	Sep	Oct	Nov	Dec
Precipitation	*RMSE*	**2.380**	**2.922**	**5.829**	**7.553**	**10.284**	**15.212**	**15.708**	**13.595**	**12.115**	**6.207**	**3.439**	**1.719**
	R^2	0.736	0.767	0.775	0.888	0.912	0.906	0.898	0.901	0.896	0.919	0.867	0.714
	MAE	1.310	1.716	3.799	5.323	7.176	10.970	11.785	10.314	9.107	4.320	1.886	0.971
Average temperature	*RMSE*	**1.242**	**1.163**	**1.132**	**0.976**	**0.936**	**0.933**	**0.824**	**0.784**	**0.857**	**0.918**	**1.049**	**1.172**
	R^2	0.936	0.948	0.939	0.961	0.944	0.942	0.956	0.963	0.954	0.946	0.951	0.922
	MAE	0.964	0.878	0.844	0.722	0.678	0.680	0.613	0.594	0.632	0.685	0.815	0.924
Maximum temperature	*RMSE*	**1.310**	**1.509**	**1.369**	**1.272**	**1.230**	**1.182**	**1.042**	**0.990**	**1.096**	**1.265**	**1.103**	**1.089**
	R^2	0.925	0.907	0.893	0.929	0.922	0.917	0.941	0.943	0.905	0.914	0.942	0.942
	MAE	0.921	1.069	1.006	0.949	0.829	0.816	0.746	0.738	0.810	0.896	0.799	0.813
Minimum temperature	*RMSE*	**1.853**	**1.566**	**1.256**	**1.062**	**0.966**	**0.963**	**0.929**	**0.961**	**0.893**	**1.119**	**1.469**	**1.799**
	R^2	0.888	0.920	0.940	0.955	0.945	0.948	0.948	0.947	0.950	0.943	0.912	0.889
	MAE	1.459	1.202	0.979	0.840	0.759	0.740	0.734	0.752	0.667	0.875	1.181	1.422

https://doi.org/10.5194/essd-2022-45
Preprint. Discussion started: 1 March 2022

Table 5. Tenfold cross-validation statistics for selected models based on independent weather stations in Temperate monsoonal region

Climate elements	Statistic indices	Jan	Feb	Mar	Apr	May	Jun	Jul	Aug	Sep	Oct	Nov	Dec
Precipitation	*RMSE*	**1.463**	**2.039**	**2.885**	**4.117**	**7.931**	**9.751**	**15.572**	**14.935**	**6.682**	**4.783**	**2.202**	**1.408**
	R^2	0.969	0.971	0.962	0.953	0.955	0.951	0.893	0.880	0.933	0.901	0.955	0.959
	MAE	0.892	1.146	1.787	2.389	4.040	5.975	10.965	10.151	4.599	2.918	1.459	0.845
Average temperature	*RMSE*	**0.732**	**0.635**	**0.457**	**0.422**	**0.434**	**0.390**	**0.326**	**0.310**	**0.402**	**0.447**	**0.526**	**0.672**
	R^2	0.989	0.990	0.991	0.986	0.977	0.978	0.981	0.984	0.983	0.988	0.991	0.990
	MAE	0.506	0.439	0.331	0.313	0.320	0.270	0.230	0.236	0.303	0.327	0.396	0.481
Maximum temperature	*RMSE*	**0.452**	**0.451**	**0.434**	**0.452**	**0.449**	**0.431**	**0.402**	**0.335**	**0.291**	**0.273**	**0.345**	**0.436**
	R^2	0.995	0.994	0.992	0.982	0.970	0.972	0.962	0.972	0.989	0.995	0.996	0.995
	MAE	0.278	0.283	0.296	0.301	0.277	0.266	0.257	0.227	0.199	0.184	0.238	0.287
Minimum temperature	*RMSE*	**1.186**	**1.066**	**0.778**	**0.735**	**0.744**	**0.625**	**0.448**	**0.492**	**0.704**	**0.775**	**0.869**	**1.059**
	R^2	0.976	0.977	0.979	0.964	0.949	0.953	0.973	0.971	0.963	0.969	0.978	0.977
	MAE	0.832	0.748	0.600	0.557	0.563	0.458	0.322	0.366	0.522	0.572	0.648	0.762

Table 6. Tenfold cross-validation statistics for selected models based on independent weather stations in Subtropical-tropical monsoonal region

Climate elements	Statistic indices	Jan	Feb	Mar	Apr	May	Jun	Jul	Aug	Sep	Oct	Nov	Dec
Precipitation	*RMSE*	**8.999**	**9.143**	**9.990**	**11.514**	**17.116**	**26.410**	**28.207**	**28.459**	**22.054**	**17.894**	**12.174**	**9.004**
	R^2	0.908	0.946	0.970	0.968	0.935	0.873	0.735	0.795	0.864	0.873	0.857	0.861
	MAE	4.288	5.184	6.591	7.786	11.144	17.158	19.239	18.265	12.566	8.600	5.289	3.699
Average temperature	*RMSE*	**0.597**	**0.632**	**0.617**	**0.530**	**0.437**	**0.369**	**0.368**	**0.355**	**0.401**	**0.474**	**0.514**	**0.566**
	R^2	0.978	0.971	0.967	0.965	0.968	0.976	0.982	0.984	0.979	0.976	0.976	0.977
	MAE	0.395	0.414	0.400	0.347	0.299	0.255	0.268	0.261	0.295	0.342	0.370	0.401
Maximum temperature	*RMSE*	**0.749**	**0.798**	**0.786**	**0.680**	**0.579**	**0.521**	**0.515**	**0.475**	**0.514**	**0.586**	**0.615**	**0.689**
	R^2	0.973	0.962	0.956	0.943	0.937	0.950	0.967	0.970	0.963	0.965	0.967	0.972
	MAE	0.458	0.499	0.490	0.430	0.368	0.334	0.345	0.315	0.345	0.371	0.401	0.439
Minimum temperature	*RMSE*	**0.702**	**0.711**	**0.695**	**0.621**	**0.490**	**0.378**	**0.408**	**0.385**	**0.441**	**0.537**	**0.638**	**0.719**
	R^2	0.969	0.966	0.960	0.962	0.970	0.978	0.978	0.982	0.975	0.968	0.967	0.965
	MAE	0.476	0.476	0.463	0.422	0.356	0.284	0.308	0.292	0.339	0.410	0.474	0.515

4.1.2 Comparison of ChinaClim_baseline with WorldClim2 and CHELSA.

To better identify the performance of ChinaClim_baseline, it was compared with two widely recognized baseline climatology surface with same spatial resolution: WorldClim2 (Fick et al., 2017) and CHELSA (Karger et al., 2017). The spatial differences and density scatter between ChinaClim_baseline and WorldClim2 as well as CHELSA for annual total precipitation, annual average temperature, January minimum temperature, and July maximum temperature were shown in Figures 4, 5, 6, and 7 respectively.

https://doi.org/10.5194/essd-2022-45
Preprint. Discussion started: 1 March 2022

Open Access Earth System Science Data Discussions

There were some obvious spatial differences between ChinaClim_baseline and WorldClim2 and CHELSA for annual total precipitation in the temperate continental region and high cold Tibetan plateau (Figure 4a and 4b). The precipitation ratios of worldclime v2/ChinaClim_baseline were less than 50% in most areas over temperate continental region and high cold Tibetan plateau, and higher than 150% in Himalayas. WorldClim2 tended to be drier than ChinaClim_baseline in many locations of temperate continental region and high cold Tibetan plateau, but tended to be wetter in Himalayas. It is worth noting that the precipitation rate was obviously more than 150% for CHELSA in the west and south of high cold Tibetan plateau, while were less than 50% in the northeast of high cold Tibetan plateau and west of temperate continental region (Figure 4b). That is, CHELSA was pretty wetter than ChinaClim_baseline in the west and south of high cold Tibetan plateau and much drier the northeast of high cold Tibetan plateau and west of temperate continental region than ChinaClim_baseline. As shown in Figure 4c and 4d, the high correlation coefficient (r) between ChinaClim_baseline and WorldClim2 (r = 0.97) and CHELSA (r = 0.92) imply that our baseline climatology surface was trustworthy. The spatial consistency between ChinaClim_baseline and WorldClim2 was higher, which may be because they used similar algorithms to generate baseline climatology surface.

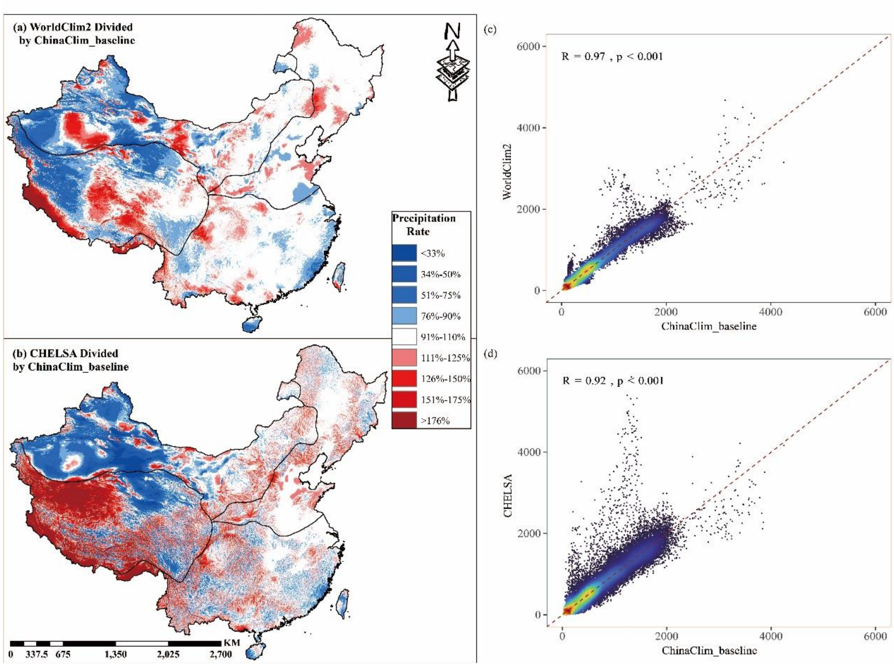

Figure 4. WorldClim2/ ChinaClim_baseline and CHELSA/ ChinaClim_baseline ratio maps (expressed as percentage) and density scatter plots of annual precipitation in China. The color of points represents the density of points, where the red points represent the highest density, and the blue points represent the lowest density. The black line is the 1:1 line.

For temperature elements (Figure 5, 6, and 7), the spatial consistent between ChinaClim_baseline and WorldClim2 as well as CHELSA were very high (the lowest r was 0.98) and the spatial discrepancy were much smaller than precipitation as temperature generally follows relatively simple gradients along latitude and elevation. Similar to precipitation, only few areas in temperate

https://doi.org/10.5194/essd-2022-45
Preprint. Discussion started: 1 March 2022

monsoonal region and subtropical-tropical monsoonal region had obvious spatial discrepancy (the areas where temperature different over 3°C), and the spatial consistent was low in temperate continental region and high cold Tibetan plateau.

Specifically, for annual average temperature, most areas showed small temperature different (< 3°C) and WorldClim2 and CHELSA were slightly hotter (red) in those areas than ChinaClim_baseline and only CHELSA in the west of high cold Tibetan plateau were colder. However, for July maximum temperature, WorldClim2 were obviously warmer than our baseline surface in the west of temperate continental region and the west of high cold Tibetan plateau, and were lower in the remaining areas. Most areas of CHELSA showed lower temperature than ChinaClim_baseline, particularly in high cold Tibetan plateau with vast high-altitude areas. Compared to other temperature elements, the spatial pattern of January minimum temperature showed much more obvious differences among our baseline surface and WorldClim2 and CHELSA (Figure 7a and 7b), but the density scatter plot (Figure 7c and 7d) showed that the correlation coefficients (*r*) were still as high as 0.99 and 0.98, respectively. Notably, obvious warmer temperature differences (red) can be captured in the eastern and southern parts of high cold Tibetan plateau both WorldClim2 and CHELSA. Furthermore, WorldClim2 in temperate continental region tended to be colder than ChinaClim_baseline, while CHELSA showed a completely opposite spatial pattern.

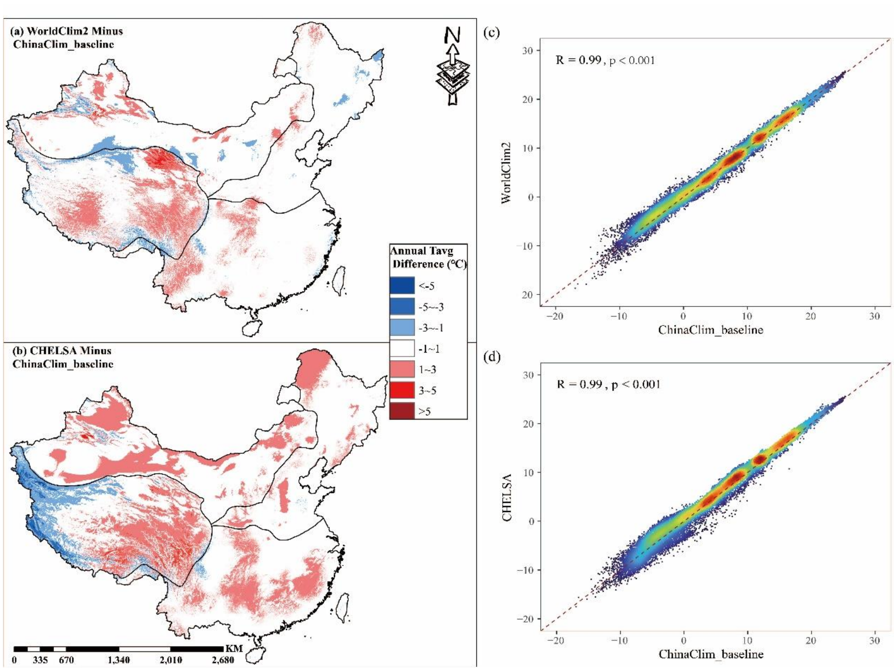

Figure 5. WorldClim2 - ChinaClim_baseline and CHELSA – ChinaClim_baseline difference maps and density scatter plots of annual average temperature in China. The color of points represents the density of points, where the red points represent the highest density, and the blue points represent the lowest density. The black line is the 1:1 line.

https://doi.org/10.5194/essd-2022-45
Preprint. Discussion started: 1 March 2022

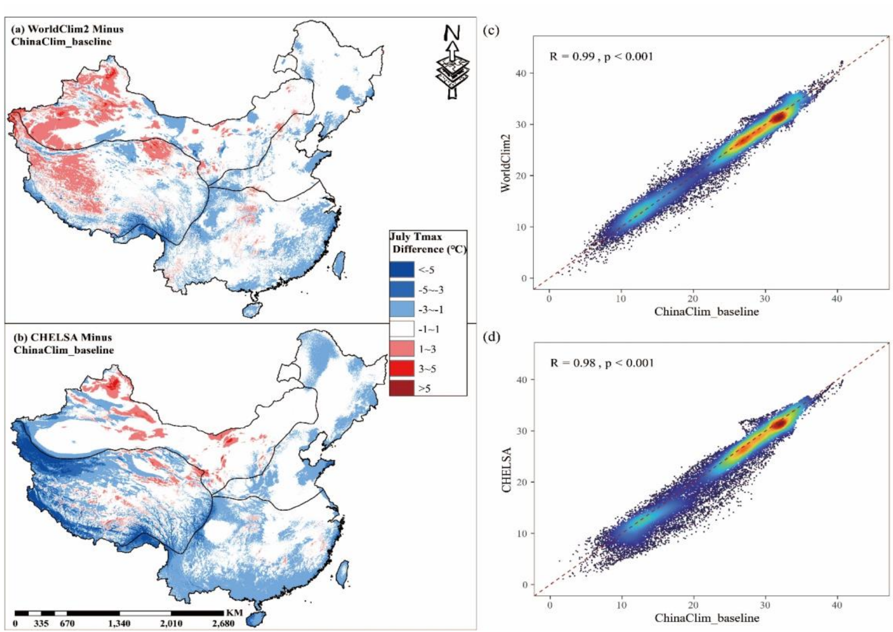

Figure 6. WorldClim2 - ChinaClim_baseline and CHELSA - ChinaClim_baseline difference maps and density scatter plots of July maximum temperature in China.

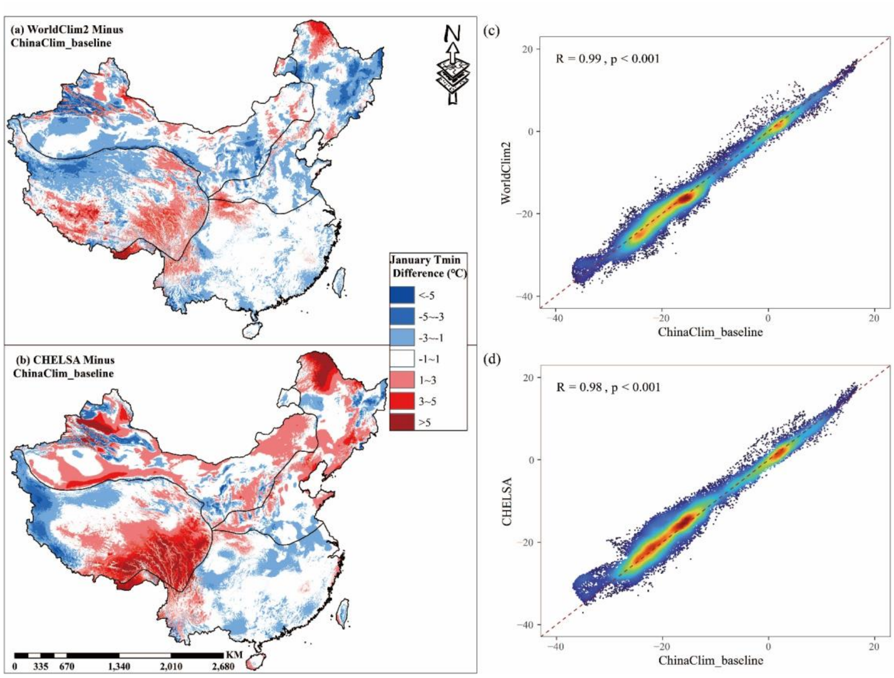

Figure 7. WorldClim2 - ChinaClim_baseline and CHELSA - ChinaClim_baseline difference maps and density scatter plots of January minimum temperature in China.

https://doi.org/10.5194/essd-2022-45
Preprint. Discussion started: 1 March 2022

4.2 1km monthly precipitation and temperatures surfaces during1952-2019 (ChinaClim_time-series)

4.2.1 The optimal models and accuracy of ChinaClim_time-series

Our results showed that Model **7** (F(x,y,z)+cru_r+base+coast / F(x,y,z)+cru_a+base+coast) had the lowest multi-year average (1952-2019) *RMSE* value in most months for precipitation and temperature elements (Table S7). Model **1** (F(x,y,z,base,coast)+cru_r / F(x,y,z,base,coast)+cru_a) also had the lowest *RMSE* in some months such as in Feb for precipitation, during Dec-Mar for average temperature and during Nov-Mar for maximum temperature. Hence, we used Model **1** and Model **7** to generate monthly climate surface in corresponding months for precipitation estimation during 1952-1997 and temperature estimation during 1952-2000. For precipitation estimation during 1998-2019 and temperature estimation during 2001-2019, models considering TRMM3B43 ratio and LST anomaly (Model **7b** and Model **1a**) showed the lowest multi-year average *RMSE* value (Table S8).

As shown in Table 4, our results demonstrated that ChinaClim_time-series showed excellent performance during 1952-2019. Precipitation had an average *RMSE* between 7.502 mm and 52.307mm, an average R^2 of 0.755~0.919, and an average of *MAE* of 4.283~36.826 mm for all months. Compared with other months, the accuracy of precipitation was slightly poor from Jun to Aug. Average temperature had an average R^2 of 0.991~0.995, an average *RMSE* between 0.461 °C and 0.731 °C, and an average *MAE* of 0.323~0.489 °C for all months. Maximum temperature had an average R^2 of 0.984~0.994, an average *RMSE* between 0.535 °C and 0.714 °C, and an average *MAE* of 0.372 °C ~ 0.485 °C for all months. Minimum temperature had an average R^2 of 0.989~0.993, an average *RMSE* between 0.547 °C and 0.939 °C, and an average *MAE* of 0.392~0.661 °C for all months. In a word, the accuracy of the average temperature was the best, followed by the maximum temperature and the minimum temperature.

Table 4. Tenfold cross-validation statistics for ChinaClim_time-series.

		Jan	Feb	Mar	Apr	May	Jun	Jul	Aug	Sep	Oct	Nov	Dec
Precipitation	*RMSE*	7.502	10.532	15.880	24.740	36.320	48.040	52.307	49.240	35.437	25.543	13.866	7.746
	R^2	0.897	0.908	0.919	0.888	0.865	0.820	0.755	0.756	0.782	0.801	0.845	0.850
	MAE	4.291	5.881	9.259	15.153	22.794	31.973	36.826	34.298	23.442	14.191	7.839	4.283
Average temperature	*RMSE*	0.731	0.682	0.565	0.480	0.463	0.461	0.466	0.467	0.493	0.506	0.607	0.717
	R^2	0.995	0.994	0.994	0.993	0.992	0.991	0.991	0.991	0.992	0.994	0.995	0.995
	MAE	0.489	0.465	0.385	0.332	0.329	0.323	0.328	0.333	0.347	0.354	0.416	0.488
Maximum temperature	*RMSE*	0.714	0.702	0.637	0.584	0.557	0.565	0.565	0.549	0.547	0.535	0.616	0.701
	R^2	0.994	0.993	0.991	0.988	0.985	0.984	0.984	0.986	0.987	0.991	0.994	0.994
	MAE	0.481	0.485	0.444	0.405	0.396	0.403	0.407	0.399	0.385	0.372	0.418	0.470
Minimum temperature	*RMSE*	0.939	0.887	0.752	0.630	0.604	0.578	0.547	0.578	0.628	0.678	0.797	0.923
	R^2	0.993	0.993	0.992	0.992	0.991	0.989	0.990	0.990	0.990	0.992	0.993	0.993
	MAE	0.661	0.633	0.539	0.459	0.441	0.411	0.392	0.413	0.453	0.495	0.573	0.655

https://doi.org/10.5194/essd-2022-45
Preprint. Discussion started: 1 March 2022

4.2.2 Comparison of ChinaClim_time-series to other datasets

Here, we compared the accuracy of ChinaClim_time-series with Peng's climate surface and CHELSAcruts by *RMSE*, R^2 and *MAE* in China and four climatic regions (Temperate continental region, High cold Tibetan Plateau, Temperate monsoonal region and Subtropical-tropical monsoonal region). The independent weather stations extracted from a tenfold cross-validation approach were used to assess the performance of ChinaClim_time-series, while only these weather stations with small deviations (< 200 m) between the recorded and actual elevation (1 km DEM) were used to assess the accuracy of CHELSAcruts and Peng's climate surface (Tables 5-7). It is worth noting that these weather stations might not be independent weather station for validating CHELSAcruts and Peng's climate surface. Thus the accuracy of CHELSAcruts and Peng's climate surface may be overestimated in this study.

Table 5. The overall accuracy of total precipitation for ChinaClim_time-series, Peng's climate surface and CHELSAcruts in China and four climatic regions during 1952-2019

		RMSE	R^2	*MAE*
China	ChinaClim_time-series	**32.867**	**0.867**	**17.716**
	Peng's climate surface	39.707	0.805	21.290
	CHELSAcruts	40.015	0.809	21.560
Temperate continental region	ChinaClim_time-series	**13.933**	**0.847**	**7.307**
	Peng's climate surface	16.575	0.791	8.881
	CHELSAcruts	15.043	0.832	7.892
High cold Tibetan Plateau	ChinaClim_time-series	**17.878**	**0.881**	**9.931**
	Peng's climate surface	31.625	0.714	16.201
	CHELSAcruts	34.228	0.696	18.000
Temperate monsoonal region	ChinaClim_time-series	**26.858**	**0.854**	**14.085**
	Peng's climate surface	29.151	0.817	15.496
	CHELSAcruts	28.819	0.831	15.375
Subtropical-tropical monsoonal region	ChinaClim_time-series	**43.626**	**0.834**	**26.662**
	Peng's climate surface	52.426	0.758	31.612
	CHELSAcruts	52.950	0.760	32.364

The precipitation accuracy of ChinaClim_time-series showed better performance than Peng's climate surface and CHELSAcruts in China and four climatic regions (Table 5) with the higher R^2 (0.867), and the lower *RMSE* (32.867 mm) and *MAE* (17.716 mm). Comparing with Peng's climate surface and CHELSAcruts, R^2 increased by 7.70 % and 7.17 %, *RMSE* decreased by 17.23 % and 17.86% and *MAE* decreased by 16.79% and 17.83 %, respectively.

Specifically, *RMSE*, R^2 and *MAE* of ChinaClim_time-series in temperate continental region were 13.933mm, 0.847 and 7.307mm, Respectively. The accuracy is higher than CHELSAcruts (*RMSE*: 15.043mm, R^2: 0.832 and *MAE*: 7.892mm), but much higher than Peng's climate surface (*RMSE*: 16.575mm, R^2: 0.791 and *MAE*: 8.881mm) in three surfaces. Remarkably, compared with Peng's climate surface and CHELSAcruts in high cold Tibetan plateau, R^2 of ChinaClim_time-series for increased by 23.39 % and 26.59 %, *RMSE* decreased by 43.47 % and 47.77 % and *MAE* decreased by 38.70 % and 44.83 %, respectively. That is, ChinaClim_time-series improved greatly

https://doi.org/10.5194/essd-2022-45
Preprint. Discussion started: 1 March 2022

precipitation accuracy in those region with low-density weather station in comparison with the other time series climate datasets. The accuracy difference of different climate datasets in temperate monsoonal region was the lower than other three climatic regions, and the *RMSE*, R^2 and *MAE* of ChinaClim_time-series was 26.858mm, 0.854 and 14.085mm, respectively. The accuracy of ChinaClim_time-series in subtropical-tropical monsoonal region were better obviously than Peng's climate surface and CHELSAcruts, and R^2 increased by 10.03 % and 9.74 %, *RMSE* decreased by 16.79 % and 17.61 % and *MAE* decreased by 15.66 % and 17.62 %, respectively.

Table 6. The overall accuracy of maximum temperature for ChinaClim_time-series, Peng's climate surface and CHELSAcruts in China and four climatic regions during 1952-2019

	Maximum temperature	*RMSE*	R^2	*MAE*
China	ChinaClim_time-series	**0.629**	**0.997**	**0.412**
	Peng's climate surface	1.299	0.988	0.974
	CHELSAcruts	1.443	0.987	1.097
Temperate continental region	ChinaClim_time-series	**0.854**	**0.996**	**0.482**
	Peng's climate surface	1.591	0.985	1.202
	CHELSAcruts	1.835	0.981	1.358
High cold Tibetan Plateau	ChinaClim_time-series	**0.676**	**0.993**	**0.473**
	Peng's climate surface	2.224	0.951	1.847
	CHELSAcruts	2.686	0.947	2.231
Temperate monsoonal region	ChinaClim_time-series	**0.483**	**0.999**	**0.352**
	Peng's climate surface	1.090	0.993	0.847
	CHELSAcruts	1.225	0.993	0.962
Subtropical-tropical monsoonal region	ChinaClim_time-series	**0.573**	**0.995**	**0.397**
	Peng's climate surface	1.252	0.978	0.935
	CHELSAcruts	1.314	0.980	1.035

Table 7. The overall accuracy of minimum temperature for ChinaClim_time-series, Peng's climate surface and CHELSAcruts in China and four climatic regions during 1952-2019

	Minimum temperature	*RMSE*	R^2	*MAE*
China	ChinaClim_time-series	**0.742**	**0.996**	**0.501**
	Peng's climate surface	1.422	0.988	1.074
	CHELSAcruts	1.523	0.987	1.125
Temperate continental region	ChinaClim_time-series	**1.016**	**0.993**	**0.673**
	Peng's climate surface	1.765	0.982	1.351
	CHELSAcruts	2.004	0.976	1.461
High cold Tibetan Plateau	ChinaClim_time-series	**0.856**	**0.992**	**0.584**
	Peng's climate surface	2.276	0.944	1.800
	CHELSAcruts	1.975	0.958	1.528
Temperate monsoonal region	ChinaClim_time-series	**0.727**	**0.997**	**0.521**
	Peng's climate surface	1.324	0.991	1.032
	CHELSAcruts	1.585	0.989	1.196
Subtropical-tropical monsoonal region	ChinaClim_time-series	**0.543**	**0.995**	**0.386**
	Peng's climate surface	1.254	0.977	0.938
	CHELSAcruts	1.119	0.984	0.878

The temperature elements accuracy of ChinaClim_time-series also showed better performance than Peng's climate surface and CHELSAcruts in China and all climatic regions (Tables 6 - 7). In whole China, the *RMSE*, R^2 and *MAE* of maximum temperature were 0.629 °C, 0.997 and 0.412 °C, respectively; the *RMSE*, R^2 and *MAE* of minimum temperature were 0.996, 0.742 °C and 0.501°C, respectively. All R^2 were very high among three datasets, but *RMSE* of ChinaClim_time-series decreased by 51.58 % (Peng's climate surface) and 56.41 % (CHELSAcruts) for maximum temperature and by 47.82% (Peng's climate surface) and 51.28 % (CHELSAcruts) for minimum temperature; *MAE* of ChinaClim_time-series decreased by 57.70 % (Peng's climate surface) and 62.44 % (CHELSAcruts) for maximum temperature and by 53.35 % (Peng's climate surface) and 55.74 % (CHELSAcruts) for minimum temperature.

The accuracy of ChinaClim_time-series also was much better than Peng's climate surface and CHELSAcruts, and the *RMSE* and *MAE* of ChinaClim_time-series reduced by about 50% in all climatic regions. Especially in high cold Tibetan plateau, the accuracy of the maximum and minimum temperature of ChinaClim_time-series were 0.676 °C and 0.856 °C for *RMSE*, 0.993 and 0.992 for R^2, and 0.473 °C and 0.584 °C for *MAE*, respectively; Compared with Peng's climate surface and CHELSAcruts, *RMSE* decreased by 69.60 % and 74.83% for maximum temperature and by 62.39 % and 56.66 % for minimum temperature, respectively; *MAE* decreased by 74.39 % and 78.80 % for maximum temperature and by 67.56 % and 61.78 % for minimum temperature, respectively.

4.2.3 The effectiveness of satellite-driven TRMM3B43 and LST

Our results have shown that models considering satellite-driven data (Table S7: Model **7b** and Model **1a**) were the best models during the periods for precipitation during 1998-2019 and for temperature elements during 2001-2019. Here, the effectiveness of satellite-driven data for improving precipitation and temperature estimation was evaluated again because simple multi-year monthly average model was difficult to quantify the influences of satellite-driven data. We investigated the accuracy of precipitation and three temperature elements with satellite-driven data and without satellite-driven data by *RMSE*, R^2 and *MAE* from density scatter plots in China (Figures 8-11) and four climatic regions (Figures S1-S4).

https://doi.org/10.5194/essd-2022-45
Preprint. Discussion started: 1 March 2022

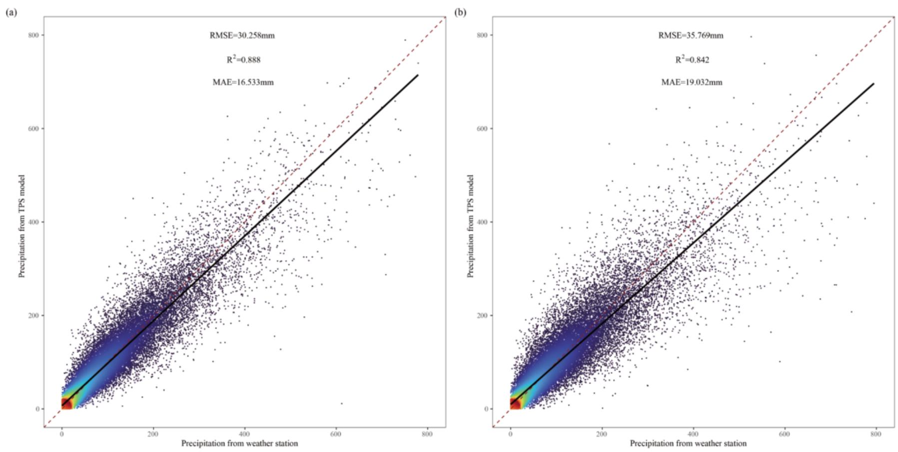

Figure 8 Density scatter plots of precipitation with satellite-driven TRMM3B43 and (b) without satellite-driven TRMM3B43 in China.

As shown in Figure 8, after considering the satellite-driven TRMM3B43, the overall *RMSE*, R^2 and *MAE* in China were 30.258mm, 0.888 and 16.533mm, but *RMSE*, R^2 and *MAE* of the model without considering the satellite-driven TRMM3B43 were 35.769mm, 0.842, and 19.032mm, respectively. Furthermore, we investigated the differences for the overall accuracy of precipitation estimation in the four climatic regions before and after adding satellite-driven TRMM3B43 (Figure S1). The results showed that *RMSE* in temperate continental region reduced from 14.798mm to 12.720mm after considering satellite-driven TRMM3B43; *RMSE* in high cold Tibetan plateau also reduced by about 2mm, from 19.831mm to 17.336mm; *RMSE* in temperate monsoonal region was 24.890mm, and decreased by 10.91 %; particularly, *RMSE* in subtropical-tropical monsoonal region reduced from 48.271mm to 40.114mm, and the reduction of *RMSE* was as high as 16.70%. In short, adding satellite-driven TRMM3B43 to TPS model can improve obviously the accuracy of precipitation estimation, whether in temperate continental region and high cold Tibetan plateau with low-density weather stations or in temperate monsoonal region and subtropical-tropical monsoonal region with huge precipitation variation.

https://doi.org/10.5194/essd-2022-45
Preprint. Discussion started: 1 March 2022

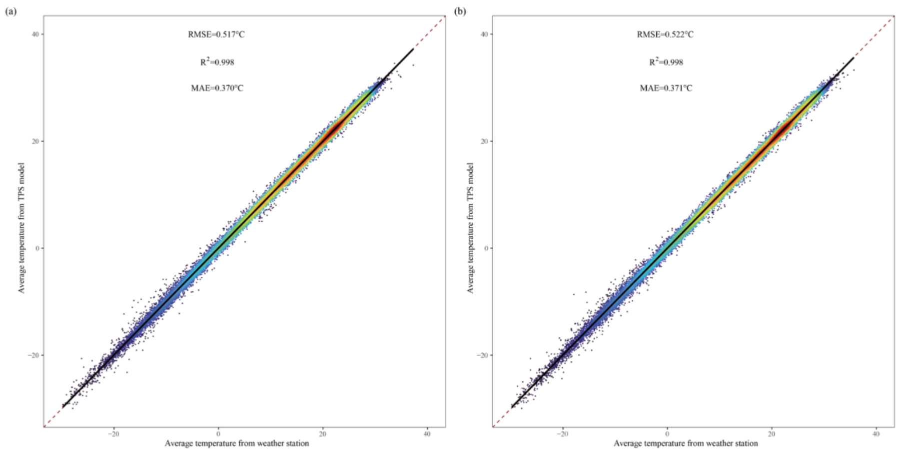

Figure 9 Density scatter plots of average temperature (a) with satellite-driven LST and (b) without satellite-driven LST in China.

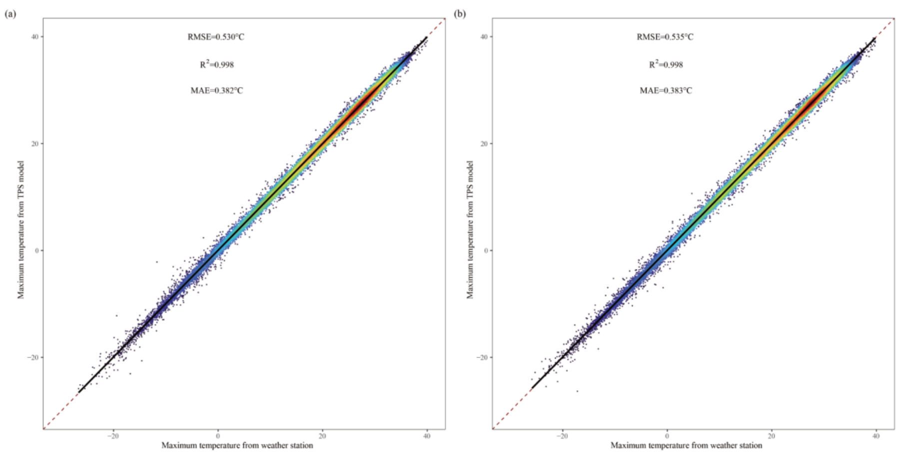

Figure 10 Density scatter plots of maximum temperature (a) with satellite-driven LST and (b) without satellite-driven LST in China.

https://doi.org/10.5194/essd-2022-45
Preprint. Discussion started: 1 March 2022

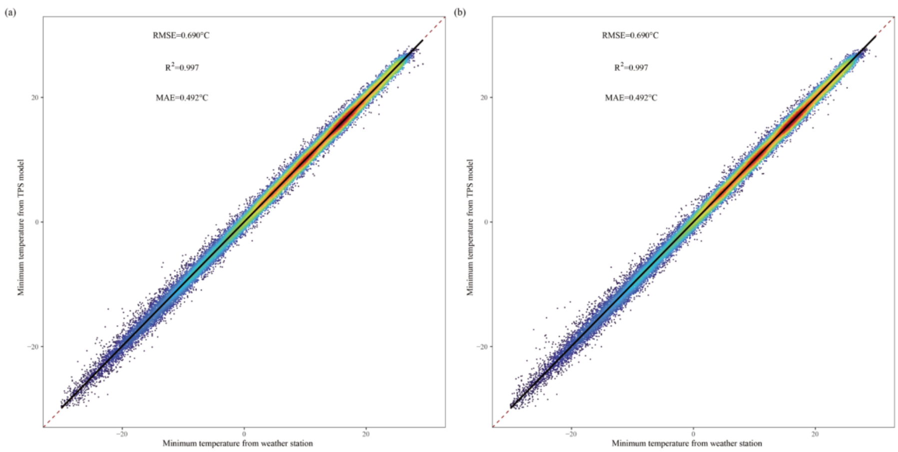

Figure 11 Density scatter plots of minimum temperature (a) with satellite-driven LST and (b) without satellite-driven LST in China.

Our results (Figures 9-11) showed that the accuracy of the temperature elements were improved slightly in China after considering satellite-driven LST. Among them, RMSE of the average temperature reduced from 0.522 to 0.517, and *RMSE* of the maximum temperature reduced from 0.535 to 0.530, the average RMSE remained unchanged. Moreover, the accuracy of temperature elements estimation in various climatic regions were not as obvious as precipitation estimation when adding satellite-driven data to the TPS model (Figures S2-S4). We inferred that temperature variation usually tends to change simply with altitude gradients, and adding CRU temperature data to the TPS model may affect the role of satellite-driven LST to the estimate of temperature elements. That is, the improvement of the accuracy of adding satellite-driven LST to TPS model for temperature elements estimation will be limited when models were able to fit the regression relationship between temperature and related variables well.

5 Data availability

ChinaClim_baseline is a brand-new and high-quality baseline climatology surface for China at spatial resolution of 1km. The data now is freely available through Zenodo at 10.5281/zenodo.5900743 (Gong, 2020a), which can be downloaded in NC format. The scale factor of precipitation and temperature are 0.01 and 0.1, respectively.
ChinaClim_time-series is a monthly temperatures and precipitation dataset in China for the period of 1952-2019 of 1km spatial resolution. The data now are freely available through Zenodo at 10.5281/zenodo.5919442 (Gong, 2020b), 10.5281/zenodo.5919423 (Gong, 2020c), 10.5281/zenodo.5919448 (Gong, 2020d), and 10.5281/zenodo.5919450 (Gong, 2020e) which can be downloaded in Geotiff format. The scale factor of the data is 0.1.

https://doi.org/10.5194/essd-2022-45
Preprint. Discussion started: 1 March 2022

6 Discussion

The high-quality climate dataset could play pivotal role in studying climate change and its effect on the processes and functioning of the ecosystem (Ordonez and Williams., 2013; Pinsky et al., 2013). However, it is difficult and expensive to build a time-series weather stations with high-density distribution network. It has been noted that more than 2000 weather stations could be freely used to generate baseline climatology surface, then our study created a brand-new and high-quality baseline climatology surface (ChinaClim_baseline) based on those weather stations (Dataset of 30-year average climate), and which were used as input to the climatologically aided interpolation (CAI), combined with available time-series weather stations, CRU datasets, and satellite-driven data to construct a time-series climate dataset (ChinaClim_time-series) with lower uncertainty.

There are a number of baseline climatology surface products for global land surface (Hijmans et al., 2005; Karger et al., 2017; New et al., 1999; New et al., 2002; Fick et al., 2017), while few weather stations from China were employed to generate these surfaces, which might result in insufficient accuracy of these surfaces in China, and further affect the accuracy of long-term climate datasets with these surfaces as input, especially in temperate continental region and high cold Tibetan plateau where weather stations were sparse. In this study, ChinaClim_baseline could greatly reduce the uncertainty of climatic elements interpolation in remote areas owing to the high-density distribution of weather stations. As our results showed that, the estimation of ChinaClim_baseline performed well in all months for four climatic regions and the *RMSEs* of precipitation and temperature elements estimation being 1.276 ~28.439 mm. and 0.310 ~ 2.040 °C, respectively. ChinaClim_baseline, as a brand-new baseline climatology surface currently released for China, was highly consistent with WorldClim2 and CHELSA (high *r*). However, ChinaClim_baseline also showed clearly spatial differences with WorldClim2 and CHELSA over China, especially in low-density weather station regions such as high cold Tibetan Plateau and temperate continental region. WorldClim2 tended to be drier than ChinaClim_baseline in many locations of temperate continental region and high cold Tibetan plateau, which may overestimate the drought risk when being applied for assessing the influence of climate changes in these areas. CHELSA simply used temperature lapse rates to estimate temperatures, which might product mistakenly temperatures estimation in the absence of sufficient weather stations correction in high-altitude regions. Although WorldClim2 considered satellite-driven LST and cloud cover, it did not optimized the fitting model of climate elements in each months (Hijmans et al., 2005; Fick et al., 2017), which might impact the accuracy of key months and cannot correctly reveal the seasonal variation of climate elements well and mislead the vegetation-climate relationship. Previous study demonstrated that local context and seasons changes has siginificant influence on climate processes (Brunsdon et al., 2001; Fick et al., 2017), thus the model for fitting baseline climatology surface should vary from various climatic regions and different months to improve the data accuracy. ChinaClim_baseline was created by the optimal TPS model for each climatic region and different months. This adaptive method allowed for better model fits in remote regions and specific months. Moreover, ChinaClim_baseline used not only much more weather stations, but also the spatially continuous satellite-driven TRMM3B43 which can distinguish the rain shadow effect of mountains (Deblauwe et al., 2016) and provide enough information in sparse areas of weather stations.

Therefore, our high-quality baseline climatology surface should better reduce the uncertainty and

https://doi.org/10.5194/essd-2022-45
Preprint. Discussion started: 1 March 2022

reflect the actual climate conditions over China than currently existing baseline climatology surface, especially in temperate continental region and high cold Tibetan plateau with sparse weather station during growing season. Beside, a good baseline climatology surface, not only could be applied in modelling history and paleo climate changes, but also can be combined with GCM products to predicting future climate change scenarios with high resolution (Peng et al., 2019; Platts et al., 2015). ChinaClim_baseline can be used to construction of more accurate bioclimatic indicators at ~1 km spatial resolution for China. Bioclimatic variables, representing annual trends, seasonality and extreme or limiting environmental factors, are much more biologically meaningful (Hijmans et al., 2005), they are more suitable for examining the vegetation-climate relationship (Liu et al.,2020; Marchi et al., 2019; Vega et al., 2017).

A variety of studies have developed many superior long-term climate data products with high resolution, such as CHELSAcruts and Peng's climate surface. They simply relied on coarse CRU anomaly and baseline climatology surfaces (WorldClim2 and CHELSA) (Karger et al., 2017; Peng et al., 2019), which maybe lead to huge uncertainty. In this study, ChinaClim_baseline as input in CAI reduced the uncertainty of output (ChinaClim_time-series). Simultaneously, we interpolated climatic elements anomaly (ratio) based on the optimal monthly TPS model, which can not only make full use of time-series weather stations, but also consider the satellites-driven data (TRMM 3B43 ratio and LST anomaly) and CRU data as either independent spline variables or linear covariates to further improve the accuracy of the final monthly climate surface. As our results showed that compared with these two climate data products, ChinaClim_time-series increased the accuracy (*RMSE*) by more than 15% and 50% for precipitation and temperature elements, respectively, especially in temperate continental region and high cold Tibetan plateau. Previous study demonstrated that satellite-driven data can effectively improve the accuracy of climatic elements interpolation. Our results showed that the utilization of satellite-driven TRMM3B43 ratio in TPS interpolation improved the precipitation estimation of ChinaClim_time-series, but satellite-driven LST anomaly did not significantly improve the estimates of time-series temperature elements. Incorporating satellite-driven LST into spline interpolation induced diminishing returns owing to increasing the number of predictor variables, and strong correlations between temperature variables and CRU predictors may be contributing to this result. Beside, since CRU data could provide long-time series climatic element information, it plays an irreplaceable role for the reconstruction of long-time series climatic element. In particular, for the estimation of temperature elements, CRU data can play the role of LST data to a certain extent, which will provide us with important guiding significance for downscaling or spatial interpolation of time-series climatic elements. That is, a high-quality baseline climatology surface based on high-density weather stations could improve the estimates of time-series climate elements, while satellite-driven data is more helpful to improve the accuracy of precipitation estimates and produce very little effect in improving the accuracy of temperatures estimation. Hence, ChinaClim_time-series, a very high-quality time-series climate elements datasets over China, can reveal successfully the spatial-temporal change patterns of precipitation and temperatures. At the same time, considering 68 years' span, it can be used to more accurately assess the prolonged effects of climate changes on eco-environment.

The TRMM3B43 improves the estimate of precipitation, while the 0.25-degree spatial resolution of TRMM might be fail to represent many important finer-scale climatic features (Deblauwe et al., 2016) due to the uncertainties caused by downscaling from 0.25 degree to 1km using Cubist algorithm although this algorithm was recommended for exploring downscaling of satellite-based data (Ma et al., 2018). It should also be noted that there is a temporal mismatch between the datasets from weather stations (1981–2010) and from average TRMM3B43 (1998-2019) in estimating ChinaClim_baseline. Therefore, incorporating TRMM3B43 into the generation of ChinaClim_baseline and ChinaClim_time-series may exist challenges (Deblauwe et al., 2016). Similarly, the 0.5-degree spatial resolution of CRU datasets was interpolated into 1km also caused uncertainties and impact the accuracy of ChinaClim_time-series. With the emergence of more climate-related remote sensing products at high-resolution in the future, and the improvement of multiple-source remote sensing data fusion technology, the uncertainty of climate interpolation were greatly reduced and the accuracy of product estimation will be improved, particularly in places with very few weather stations or strong gradients change or complex terrain (Immerzeel et al., 2009; Li and Shao, 2010; Fick et al., 2017; Vega et al 2017). Although our research showed that TPS method could be used well in climate interpolation, this method accounted for direct elevation effects only, and had difficulty in considering the sharp changes in the relationship between climate and elevation (Daly et al., 2008; Daly et al., 2007; Marchi et al., 2019). Therefore, it is essential to comprehensively quantify the non-linear relationship between environmental variables and climate elements, and more deeply understand the impact of the interaction among environmental variables on climate elements. It is urgently needed in future work to couple the nonlinear relationship and variables interactions in climate elements interpolation with TPS or new algorithm for the better climate elements estimations.

Author Contributions. Haibo Gong formed the original idea and wrote the original manuscript; Huiyu Liu offered valuable comments and was responsible for the manuscript revisions; Xueqiao Xiang participated in the data collection and analysis; FuSheng Jiao and Xiaojuan Xu created figures and tables.

Competing interests. The author declare that they have no conflict of interest.

Acknowledgements. We thank the all people and institutions who contributed to the establishment of this dataset.

Financial support. This research had been funded by the National Natural Science Foundation of China (No. 41971382, 31870454) and the Priority Academic Program Development of Jiangsu Higher Education Institutions (164320H116).

References

Abatzoglou, J.T., Dobrowski, S.Z., Parks, S.A., and Hegewisch, K.C.: TerraClimate, a high-resolution global dataset of monthly climate and climatic water balance from 1958–2015, Scientific Data., 5,170191, 2018.

Becker, A., et al.: A description of the global land-surface precipitation data products of the Global Precipitation Climatology Centre with sample applications including centennial (trend) analysis from 1901–present, Earth System Science Data., 5,1(2013-02-21), 5(1), 921-998, 2013.

Belda, M., Holtanova, E., Kalvova, J., and Halenka, T.: Global warming-induced changes in climate region based on CMIP5 projections, Climate Research., 71(1), 17-31, 2017.

https://doi.org/10.5194/essd-2022-45
Preprint. Discussion started: 1 March 2022

Biasutti, M., Yuter, S.E., Burleyson, C.D., and Sobel, A.H.: Very high resolution rainfall patterns measured by TRMM precipitation radar: seasonal and diurnal cycles, Climate Dynamics., 39(1), 239-258, 2012.

Boer, E.P.J., Beurs, K.M.de., and Hartkamp, A.D.: Kriging and thin plate splines for mapping climate variables, International Journal of Applied Earth Observation and Geoinformation., 3(2), 146-154, 2001.

Vega, G.C., Pertierra, L.R., and Olalla-Tárraga, M.Á.: MERRAclim, a high-resolution global dataset of remotely sensed bioclimatic variables for ecological modelling, Scientific Data., 4(1), 170078, 2017.

Chaney, N.W., Sheffield, J., Villarini, G., and Wood, E.F.: Development of a High-Resolution Gridded Daily Meteorological Dataset over Sub-Saharan Africa: Spatial Analysis of Trends in Climate Extremes, Journal of Climate., 27(15), 5815-5835, 2014.

Chen, Y., et al.: A new downscaling-integration framework for high-resolution monthly precipitation estimates: Combining rain gauge observations, satellite-derived precipitation data and geographical ancillary data, Remote Sensing of Environment., 214, 154-172, 2018.

Daly, C., Gibson, W.P., Taylor, G.H., Johnson, G.L., and Pasteris, P.: A knowledge-based approach to the statistical mapping of climate, Climate Research., 22(2), 99-113, 2002.

Daly, C., et al.: Physiographically sensitive mapping of climatological temperature and precipitation across the conterminous United States, International Journal of Climatology., 28(15) , 2008.

Daly, C., Smith, J.W., Smith, J.I., and Mckane, R.B.: High-Resolution Spatial Modeling of Daily Weather Elements for a Catchment in the Oregon Cascade Mountains, United States, Journal of Applied Meteorology & Climatology., 46(10): 1565-1586, 2007.

Deblauwe, V., et al.: Remotely sensed temperature and precipitation data improve species distribution modelling in the tropics, Global Ecology & Biogeography; 25(4): 443-454, 2016.

Gao, L., et al.: A high-resolution air temperature data set for the Chinese Tian Shan in 1979–2016, Earth Syst. Sci. Data., 10(4): 2097-2114, 2018.

Gong, H.: A Brand-New and High-Quality Baseline Climatology Surface for China (ChinaClim_baseline) [Data set]. Zenodo. https://doi.org/10.5281/zenodo.5900743, 2020a

Gong, H.: 1 km Monthly Precipitation Dataset for China from 1952 to 2019 (ChinaClim_time-series) [Data set]. Zenodo. https://doi.org/10.5281/zenodo.5919442, 2020b

Gong, H.: 1 km Monthly Maximum Temperature Dataset for China from 1952 to 2019 (ChinaClim_time-series) [Data set]. Zenodo. https://doi.org/10.5281/zenodo.5919448, 2020c

Gong, H.: 1 km Monthly Minimum Temperature Dataset for China from 1952 to 2019 (ChinaClim_time-series) [Data set]. Zenodo. https://doi.org/10.5281/zenodo.5919423, 2020d

Gong, H.: 1 km Monthly Average Temperature Dataset for China from 1952 to 2019 (ChinaClim_time-series) [Data set]. Zenodo. https://doi.org/10.5281/zenodo.5919450, 2020e

Gustavsson, T.R., Karlsson, M., Bogren, J.R., and Lindqvist, S.: Development of Temperature Patterns during Clear Nights, J. Appl. Meteorol., 37(6): 559-571, 1998.

Hamann, A., Roberts, D.R., Barber, Q.E., Carroll, C., and Nielsen, S.E.: Velocity of climate change algorithms for guiding conservation and management, Glob. Change Biol., 21(2): 997-1004, 2015.

Harris, I., Jones, P.D., Osborn, T.J., and Lister, D.H.: Updated high-resolution grids of monthly climatic observations - the CRU TS3.10 Dataset, International Journal of Climatology., 34(3): 623-642, 2014.

Hartkamp, A.D., De Beurs, K., Stein, A., and White, J.W.: Interpolation Techniques for Climate Variables Interpolation., 1999.

Hijmans, R.J., Cameron, S.E., Parra, J.L., Jones, P.G., and Jarvis, A.: Very high resolution interpolated climate surfaces for global land areas, International Journal of Climatology., 25(15): 1965-1978, 2005.

Huffman, G.J., Adler, R.F., Bolvin, D.T., and Nelkin, E.J.: The TRMM Multisatellite Precipitation Analysis (TMPA): Quasi-Global, Multiyear, Combined-Sensor Precipitation Estimates at Fine Scales. j hydrometeor., 2010.

Hutchinson, M.F.: Interpolating mean rainfall using thin plate smoothing splines. International Journal of Geographical Information Systems, 9(4): 385-403, 1995.

Hutchinson, M.F, Xu T.: *ANUSPLIN Version 4.4 User Guide*. Australian National University: Canberra., 2013.

Immerzeel, W.W., Rutten, M.M., and Droogers, P.: Spatial downscaling of TRMM precipitation using vegetative response on the Iberian Peninsula, Remote Sensing of Environment., 113(2): 362-370, 2009.

Jin, M., and Dickinson, R.E.: Land surface skin temperature climatology: benefitting from the strengths of satellite observations, Environmental Research Letters., 5(4): 44004, 2010.

Karger, D.N., et al.: Climatologies at high resolution for the earth's land surface areas, Scientific Data., 4(1),170122, 2017.

Kilibarda, M., et al.: Spatio-temporal interpolation of daily temperatures for global land areas at 1 km resolution, Journal of Geophysical Research: Atmospheres., 119(5), 2294-2313, 2014.

Kolios, S., and Kalimeris, A.: Evaluation of the TRMM rainfall product accuracy over the central Mediterranean during a 20-year period (1998–2017), Theoretical and Applied Climatology., 139(1): 785-799, 2020.

Lawrimore, J.H., et al.: An overview of the Global Historical Climatology Network monthly mean temperature data set, version 3, Journal of Geophysical Research Atmospheres., 116(D19), 2011.

Li, M., and Shao, Q.: An improved statistical approach to merge satellite rainfall estimates and raingauge data, Journal of Hydrology., 385(1-4): 51-64, 2010.

Liu, H., Jiao, F., Yin, J., Li, T., Gong, H., Wang, Z., and Lin, Z.: Nonlinear relationship of vegetation greening with nature and human factors and its forecast - A case study of Southwest China, Ecological Indicators., 111, (2020): 106009.

Liu, Q., et al.: The hydrological effects of varying vegetation characteristics in a temperate water-limited basin: Development of the dynamic Budyko-Choudhury-Porporato (dBCP) model, Journal of Hydrology., 595-611, 2016.

Marchi, M., Sinjur, I., Bozzano, M., and Westergren, M.: Evaluating WorldClim Version 1 (1961-1990) as the Baseline for Sustainable Use of Forest and Environmental Resources in a Changing Climate, Sustainability., 11(11): 14, 2019.

Michaelides, S., et al.: Precipitation: Measurement, remote sensing, climatology and modeling, Atmospheric Research., 94(4): 512-533, 2009.

Mildrexler, D.J., Zhao, M., and Running, S.W.: A global comparison between station air temperatures and MODIS land surface temperatures reveals the cooling role of forests. 116(G3) , 2011.

Mosier, T.M., Hill, D.F., and Sharp, K.V.: 30-Arcsecond monthly climate surfaces with global land coverage, International Journal of Climatology., 34(7) , 2014.

Muller, R.A., Rohde, R., Jacobsen, R., Muller, E., and Wickham, C.: A New Estimate of the Average Earth Surface Land Temperature Spanning 1753 to 2011, 2013.

New, M., Hulme, M., and Jones, P.: Representing Twentieth-Century Space–Time Climate Variability. Part I: Development of a 1961–90 Mean Monthly Terrestrial Climatology, Journal of Climate., 12(3): 829-856, 1999.

New, M., Lister, D., Hulme, M., and Makin, I.: A high-resolution data set of surface climate over global land areas, Climate Research., 21(1): 1-25, 2002.

Ordonez, A., and Williams, J.W.: Projected climate reshuffling based on multivariate climate-availability, climateanalog, and climate-velocity analyses: Implications for community disaggregation, Climatic Change., 119(3-4): 659–675, 2013.

Parmentier, B., et al.: An Assessment of Methods and Remote-Sensing Derived Covariates for Regional Predictions of 1 km Daily Maximum Air Temperature, Remote Sensing., 6(9): 8639-8670, 2014.

Peng, S., Ding, Y., Liu, W., and Li, Z.: 1 km monthly temperature and precipitation dataset for China from 1901 to 2017, Earth Syst. Sci. Data., 11(4): 1931-1946, 2019.

Peng, S., et al.: Spatiotemporal change and trend analysis of potential evapotranspiration over the Loess Plateau of China during 2011–2100, Agricultural and Forest Meteorology., 233: 183-194, 2017.

Pfister, L., et al.: Statistical reconstruction of daily precipitation and temperature fields in Switzerland back to 1864, Clim. Past., 16(2): 663-678, 2020.

https://doi.org/10.5194/essd-2022-45
Preprint. Discussion started: 1 March 2022

Platts, P.J., Omeny, P.A., and Marchant, R.: AFRICLIM: high-resolution climate projections for ecological applications in Africa, African Journal of Ecology., 53(1), 103-108, 2015.

Pinsky, M.L., Worm, B., Fogarty, M.J., Sarmiento, J.L., and Levin, S.A.: Marine taxa track local climate velocities. Science (New York, N.Y.)., 341(6151): 1239–1242, **2013**.

Ray, D., et al.: Comparing the provision of ecosystem services in plantation forests under alternative climate change adaptation management options in Wales, Reg. Envir. Chang., 15(8): 1501-1513, 2015.

Simpson, J., Kummerow, C., Tao, W.K., and Adler, R.F.: The Tropical Rainfall Measuring Mission (TRMM) Sensor Package, Meteorology & Atmospheric Physics., 60(1-3): 19-36, 1996.

Siuki, S.K., Saghafian, B., and Moazami, S.: Comprehensive evaluation of 3-hourly TRMM and half-hourly GPM-IMERG satellite precipitation products, International Journal of Remote Sensing., 38(1-2): 558-571, 2017.

Fick, S.E., and Hijmans, R.J.: WorldClim 2: new 1-km spatial resolution climate surfaces for global land areas, International Journal of Climatology., 37(12), 4302-15, 2017.

Sterl, A., Komen, G.J., and Cotton, P.D.: Fifteen years of global wave hindcasts using winds from the European Centre for Medium-Range Weather Forecasts reanalysis: Validating the reanalyzed winds and assessing the wave climate, Journal of Geophysical Research Oceans., 103, 5477-5492, 1998.

Thornton, P.E., Running, S.W., and White, M.A.: Generating surfaces of daily meteorological variables over large regions of complex terrain, Journal of Hydrology., 190(3-4): 214-251, 1997.

Willmott, C.J., and Robeson, S.M.: Climatologically aided interpolation (CAI) of terrestrial air temperature, International Journal of Climatology., 15(2), 2010.

Wu, T., and Li, Y.: Spatial interpolation of temperature in the United States using residual kriging, Applied Geography., 44: 112-120, 2013.

Yao, R., Wang, L., Huang, X., Li, L., and Jiang, W.: Developing a temporally accurate air temperature dataset for Mainland China, Science of The Total Environment., 706, 136037, 2020.